Space Sci Rev (2020) 216:22
https://doi.org/10.1007/s11214-020-0638-2

Entry System Technology Readiness for Ice-Giant Probe Missions

Ethiraj Venkatapathy[1] · Donald Ellerby[1] · Peter Gage[2] · Dinesh Prabhu[3] · Matthew Gasch[1] · Cole Kazemba[1] · Charles Kellerman[4] · Sarah Langston[5] · Benjamin Libben[3] · Milad Mahzari[1] · Frank Milos[1] · Alexander Murphy[3] · Owen Nishioka[1] · Keith Peterson[1] · Carl Poteet[5] · Scott Splinter[5] · Margaret Stackpoole[1] · Joseph Williams[3] · Zion Young[1]

Received: 7 July 2019 / Accepted: 26 January 2020 / Published online: 25 February 2020

Abstract NASA has successfully developed a new and innovative Heatshield for Extreme Entry Environments Technology, or HEEET, which, at a Technology Readiness Level (TRL) of 6, is ready for use in Ice Giant missions. HEEET is not just a replacement for the legacy full-density carbon-phenolic (FDCP) material, which was used in NASA's Pioneer-Venus and Galileo missions; it is also a more mass efficient and robust alternative, and a technology that has a sustainable manufacturing base. HEEET is a dual-layer, 3-dimensionally woven material. It has a dense outer layer, made of pure carbon fibers, that comes into contact with and protects against extreme entry environments. Below this layer is an integrally woven, lower density insulating layer, made of a blend of carbon and phenolic yarn, that reduces heat-conduction to the carrier structure. The present paper describes development of this material, its thermal, structural, and aerothermal testing, production of an engineering test unit at flight scale, and maturation for infusion into missions to various planetary destinations, with a focus on Ice Giant *in situ* missions. Finally, for representative entry velocities at Uranus and Neptune, and a range of entry masses and flight path angles, margined thicknesses of HEEET are computed. When the limits of heat fluxes and pressures that can be achieved in ground-test facilities, and loom limits, are imposed on these thickness estimates, it is shown that several atmospheric entry missions are possible at the two destinations.

Keywords Ice giants · Atmospheric entry · Entry system · Thermal protection system · Ablative material · 3D woven material · Carbon-phenolic

In Situ Exploration of the Ice Giants: Science and Technology
Edited by Olivier J. Mousis and David H. Atkinson

✉ E. Venkatapathy

1 NASA Ames Research Center, Moffett Field, CA, USA

2 Neerim Corporation, Moffett Field, CA, USA

3 AMA Inc. at NASA Ames Research Center, Moffett Field, CA, USA

4 Jacobs Technology, Inc. at NASA Johnson Space Center, Houston, TX, USA

5 NASA Langley Research Center, Hampton, VA, USA

Abbreviations

ETU: Engineering Test Unit
FDCP: Full-density carbon-phenolic
FEM: Finite element method
HCP: Heritage carbon-phenolic
HEEET: Heatshield for Extreme Entry Environments Technology
IHF: Interaction Heating Facility
IGP: Ice Giant probes
IL: Insulation Layer
PDR: Preliminary Design Review
PICA: Phenolic-Impregnate Carbon-Phenolic
RL: Recession Layer
SEP: Solar-Electric Propulsion
TPS: Thermal protection system
TRL: Technology Readiness Level

1 Introduction

The structure and composition of the atmospheres of the Outer Planets—Jupiter, Saturn, Uranus, and Neptune—are important for understanding the formation and evolution of the solar system. With the sole exception of Jupiter, for which *in situ* atmospheric measurements were made by NASA's successful Galileo probe in 1995, all of these atmospheres have been studied only through flybys of NASA's Voyager 1 and Voyager 2 robotic spacecraft. In the early 1970s Sullivan et al. (1972) made the case for *in situ* scientific study of the atmospheres of Uranus and Neptune using entry probes, and Tauber (1971) and Mezines (1974) presented approaches using carbon-phenolic as the ablative material to protect the science payloads against atmospheric entry aeroheating environments. There have been few other studies (Vojvodich et al. 1975; Tauber et al. 1994; Atreya et al. 2006; Hubbard 2011; Agrawal et al. 2014) related to Ice Giant probe missions. All these studies, while useful as point designs, do not provide a range of entry environments (peak heat flux, pressure, shear stress) required to assess the capability range of the thermal protection system (TPS), which is an integral part of the atmospheric entry system. Strictly speaking, a robust entry system would be designed with sufficient margins to accommodate not only uncertainties in atmospheric structure and composition, but other uncertainties arising from launch opportunity, arrival velocity, entry flight path angle, the mass and the size of the entry system.

The entry system used in the Galileo mission shared characteristics with that used in NASA's successful Pioneer-Venus mission which preceded it in 1978 (see Fig. 1). These two entry systems, while dissimilar in size, were similar in shape: they both had a spherically-blunted 45° cone forward aeroshell and a spherical segment backshell. The aeroshell housed a descent probe containing the science instruments; the descent probe was pressurized in the case of Pioneer-Venus and was vented in the case of Galileo. The descent probes were attached to a parachute that was deployed at subsonic conditions (at the end of the heat pulse) when the forward heatshield was jettisoned. Both entry systems used a full density carbon-phenolic (FDCP) material, or simply, heritage carbon-phenolic (HCP), for the forward heatshield. Given the proven performance of HCP, almost all of the early studies for *in situ* missions to Uranus and Neptune were predicated upon the use of this material for heatshielding.

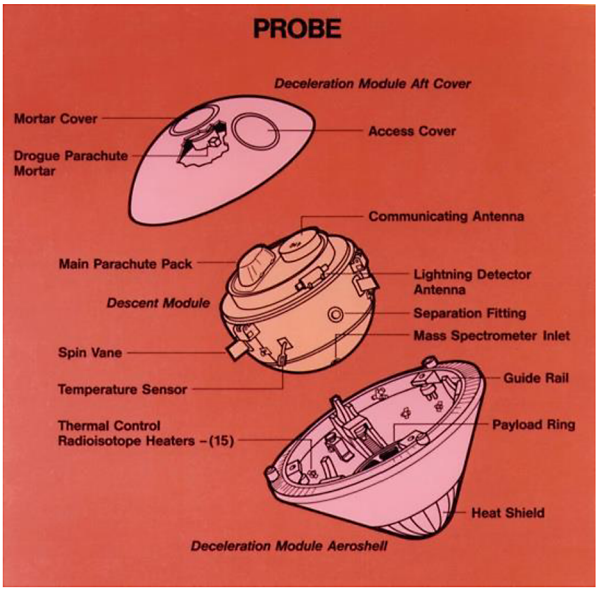

Fig. 1 The Galileo entry system consists of the descent module that contained all the science instruments, the heatshield, the aft cover and the parachute

The most comprehensive Ice Giants mission design study performed to date is the NASA-funded study led by JPL (Hofstadter et al. 2017). This pre-decadal study considered science goals and notional instruments to achieve them, and also assessed the technology readiness of various elements of missions to the Ice Giants. Although the study did not call out a specific mission to fly, 4 out of the 6 recommended architectures had an atmospheric entry probe element: (i) a Uranus orbiter with a probe, with and without the use of SEP in interplanetary travel, (ii) a Uranus flyby with a probe, and (iii) a Neptune orbiter with a probe, with the use of SEP in interplanetary travel. Not surprisingly, the atmospheric entry system design drew on heritage from the Galileo probe. The entry system consisted of a 45° sphere-cone heatshield scaled down from 1.23 m (Galileo) to 1.2 m in diameter, and a spherical backshell. The proposed design had margined mass of 321.5 kg for the entry system, which is comparable with the 335 kg entry mass of Galileo. Table 1 provides estimates of peak heat fluxes and pressures at the stagnation point and the corresponding total heat loads for the 5 point designs considered in the study. An important conclusion from the study, and one relevant to the present paper, was that while the structure, backshell TPS, and parachutes (drogue and main), were readily available, having been used successfully in many recent missions, the only subsystem that required special attention was the heatshield. For the atmospheric entry probe, therefore, two thermal protection options were considered for the forward heatshield: (i) HCP, and (ii) HEEET, which was still under development during the study. Despite the early stage of development of HEEET, the study found that HCP would be too heavy and recommended the more mass efficient HEEET material as an enabler for Ice Giant missions. These conclusions were based on just 5 point designs using a very preliminary assessment of the HEEET material.

Following the comprehensive Ice Giants study, NASA initiated another study (Hwang 2018) to explore the idea of a common probe architecture that could be used for *in situ* missions to various destinations—Venus, Saturn, Uranus and Neptune. While this follow-on study considered entry trajectories for all four planets for a common probe design, it considered only two entry flight path angles for each destination—a "shallow" one to limit

Table 1 Entry environments for Uranus and Neptune missions considered in the pre-decadal study (Hofstadter et al. 2017)

Planet	Uranus		Neptune		
Entry parameters	Design #1	Design #2	Design #3	Design #4	Design #5
Hyperbolic excess velocity (km/s)	9.91	8.41	1232	11.3	11.4
Inertial entry velocity (km/s)	23.1	22.52	26.12	25.73	25.72
Inertial entry flight path angle (deg)	−35	−30	−34	−20	−16
Inertial heading angle (deg)	−5.82	−20.02	−99.1	−84.26	−86.45
Latitude (deg)	−9.22	−5.63	−1.42	24.8	22.64
Max deceleration (g load)	216.65	164.75	454.91	208.71	124.51
Stg pressure (bar)	12	9	25	11.5	6.8
Peak convective heat flux (W/cm^2)	3456	2498	9368.5	5362.4	4311
Peak radiative heat flux (W/cm^2)	0	0	265.68	99.12	68.2
Peak total heat flux (W/cm^2)	3456	2498	9634	5462	4379
Total heat load (J/cm^2)	43572	41114	81476	109671	133874
HCP TPS mass (kg)	*Not computed*	29	*Not computed*	39	47
HEEET TPS mass (kg)		60		73	88
Feasible design	Maybe	Yes	No	Maybe	Maybe

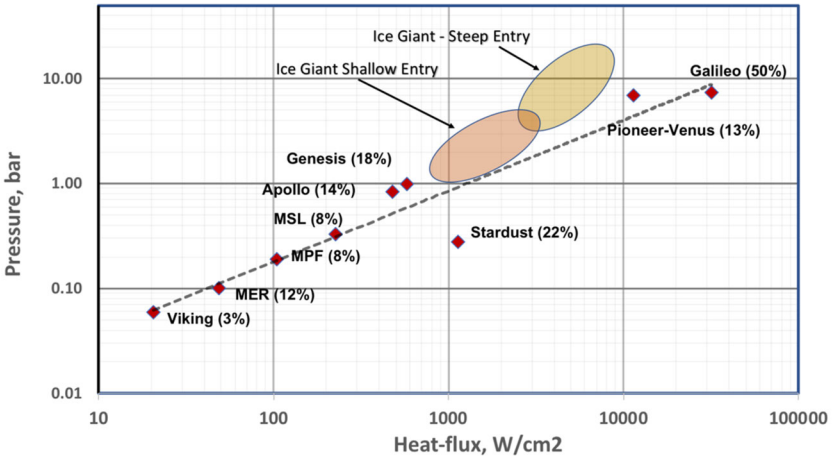

Fig. 2 Historical missions and peak entry conditions that heatshields were designed to with stand. Note the axes are in log scale

deceleration loads to 50 g, and a "steep" one that permits deceleration loads up to 150 g. All entry flight path angles were shallow relative to those used in the pre-decadal study.

The range of peak heat fluxes and stagnation pressures from these previous Ice Giants studies for various combinations of relative entry velocity, entry flight path angle, and ballistic coefficient ($\beta = m/C_D S$, where β, m, C_D, and S, are, respectively, the ballistic coefficient, mass, drag coefficient, and cross sectional area of the entry system)—the three main parameters which affect the entry environments at the stagnation point of the entry system—are compared in Fig. 2 against the values from several past NASA missions; the

values shown in parentheses for each mission are the mass fraction of the TPS expressed as a percentage of the total entry mass. It is clear from the figure that there is a capability gap for a robust and mass-efficient TPS that can operate between 1000 W/cm^2 and 10000 W/cm^2; the lower limit is representative of NASA's successful Stardust mission, which used a low density phenolic-impregnated carbon ablator (PICA), and the upper limit is representative of NASA's successful Pioneer-Venus and Galileo missions, which used full density heritage carbon phenolic (HCP). It should be noted that nose radius is a fourth parameter that affects the heating at the stagnation point but not the pressure. A relatively blunt nose radius will result in lower heat flux because the convective heat flux varies inversely with the square root of the nose radius. At Uranus and Neptune, blunting the nose might be useful because the surface heating from shock layer radiation is negligible. Therefore, in addition to the cross-section area (or base diameter), the nose radius is an important parameter that should be selected judiciously.

High priority missions for NASA for the decade 2013–2022 (see National Research Council publication *Visions and Voyages* 2011), selected by the US National Research Council, include *in situ* missions to Venus, Saturn and Ice Giants. These *in situ* missions require a mass efficient ablative TPS that is robust across a broad range of entry environments. Since the process for manufacture of HCP for NASA-specific use had atrophied, NASA conducted two workshops in 2010 and 2012 to assess the status of HCP redevelopment and its use for the recommended missions. The conclusions from the Decadal Survey and the NASA workshops was that an alternate to HCP was desirable. During this period, researchers at NASA's Ames Research Center were investigating 3-D weaving of carbon and other fibers as a way to produce multi-layer ablative TPS, which appeared to be suitable for missions to Venus, Saturn, Uranus, Neptune and high-speed sample return missions to Earth. The HEEET development project grew out of these early efforts, with a goal to deliver a system for extreme environments that could perform shallow entries, with peak deceleration less than 50 g, with a thermal protection mass 40–50% lower than HCP mass for the same mission.

In the sections that follow, some details of the development of HEEET and its manufacture are presented, along with results of testing at the element, component, and subsystem level. The maturation of HEEET for infusion into missions to various planetary destinations, with a focus on *in situ* missions to the Ice Giants, is described. Finally, for representative entry velocities at Uranus and Neptune, and a range of entry masses and flight path angles, it is shown that several atmospheric entry missions are possible at the two destinations after factoring in loom capability and aeroheating environments that can be achieved in NASA's ground-test facilities.

2 Heatshield for Extreme Entry Environments Technology (HEEET)

2.1 Overview

Previous missions that used HCP flew trajectories with steep entry angles. Steep entries have intense heating pulses, but over a short time duration. Heritage carbon-phenolic is particularly suited for such high heat fluxes. Unfortunately, steep entries also generate very high deceleration, which is challenging for qualifying instruments. If deceleration loads are a major concern, then the entry can be made shallow, which spreads a heat pulse over lower peak magnitude over a longer time, and increases the total heat load HCP is not particularly efficient at such conditions, because its high thermal conductivity carries a substantial fraction of the total heat into the protective layer. Hence a thicker layer is needed to keep the

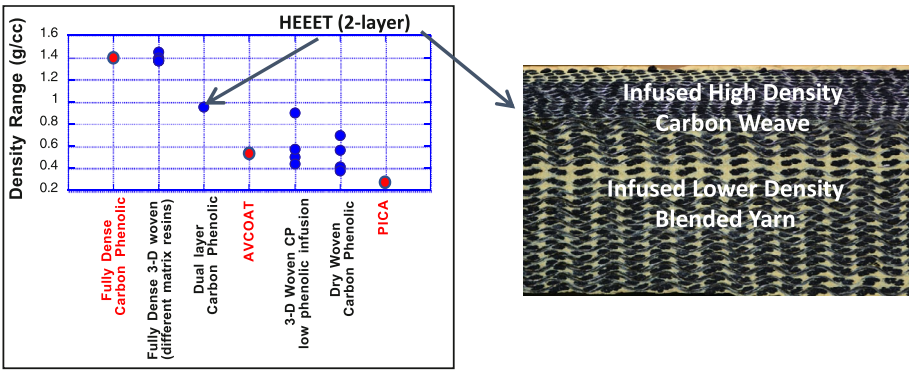

Fig. 3 (Left) Family of TPS materials manufactured using 3D weaving with resin infusion and tested with densities ranging from (0.4 g/cc–1.4 g/cc). The exploration allowed testing un-infused preforms (lowest densities) as well. (Right) dual-layer HEEET

payload at an acceptable temperature, and the TPS mass is increased. An efficient TPS that is as robust as HCP but allows shallow entry is attractive for expanding the mission design space in terms of both velocity and entry flight path angle. In 2007–2008, an ablative system that combined PICA, a low-density ablator, as an outer layer, and shuttle tile, with low conductivity, as the inner layer, was investigated for use in low to moderate entry environments (Zell et al. 2010). This investigation gave insight into the potential general advantages of a dual layer ablative system, which motivated investigation of three-dimensional woven material for extreme environments.

Three-dimensional weaving provides mechanical interlocking between layers, so through-thickness strength is much greater than stacked 2D plies, which rely on resin for layer to layer attachment. Furthermore, distinct layers can be created without relying on an adhesive to join them, by using different fibers and different weave patterns at different locations through the thickness of the integrally-woven material. Since resin selection is not governed by the need to provide inter-layer strength, resin type and infusion level can be tailored to deliver the desired ablation and internal conduction properties of the virgin and charring system characteristics.

Results from early assessments of multiple yarns and infusion levels are summarized in Fig. 3. Single and multiple layer weaves using carbon, quartz, kynol (phenolic yarn) and other blended yarns were manufactured. Infusion densities ranged from zero (no infusion) to low, moderate and full density using a variety of processes. Limited arc jet tests and property measurements showed some of these systems were very promising. A two-layer system was down selected as the 3D woven architecture of choice for both robustness end efficiency.

The dual-layer system of HEEET is made of high-density carbon “Recession Layer” (RL) at the top, to maintain low recession rate, and a lower density “Insulation Layer” (IL) below it, which uses phenolic and carbon blended yarn, at much lower density, for efficient insulation. Both layers are infused with phenolic resin at low density, using processes similar to those applied for PICA production. While it is possible to achieve a little more performance with more layers and/or density gradients, such an approach would increase complexity for characterization, manufacturing, testing and flight design. The two-layer system was determined to be a good balance of performance against development cost and system complexity.

The constituents of HEEET and HCP are primarily carbon and phenolic. The performance of both systems is affected by atmospheric chemical composition: CO_2 is an oxidiz-

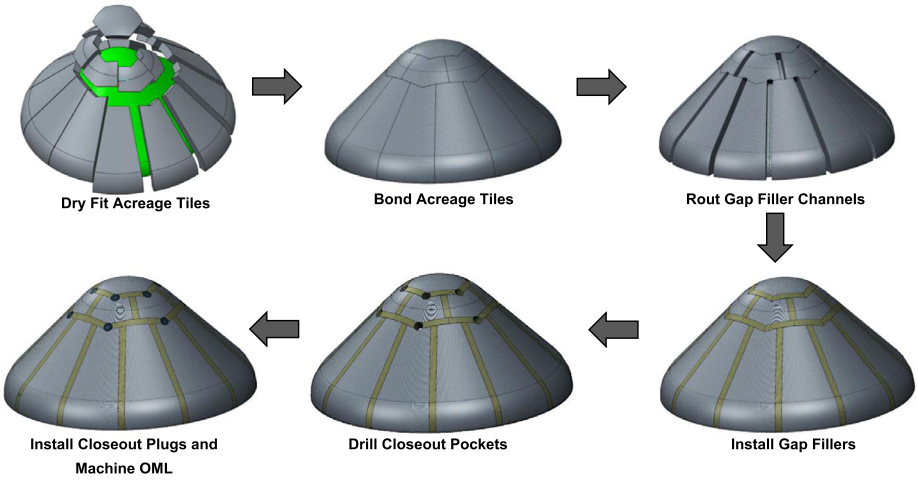

Fig. 4 Scalable tiled heatshield with seam architecture development. Flat dual-layer preforms are molded to shape, resin infused, machined and bonded to the structure A seam is essentially the same material as the acreage, but more compliant via microcracks in the phenolic. Its aerothermal behavior is the same as that of the acreage

ing environment while H_2/He is a reducing environment. Promising exploratory manufacturing, testing and mission studies indicated that HEEET should be feasible and efficient, so the HEEET project was funded to fully develop and deliver a mature heatshield technology for mission infusion

2.2 On Technology Readiness and Technology Readiness Assessment

Competitive opportunities offered by NASA's Science Mission Directorate, such as Discovery and New Frontiers, typically require new technologies to be at a Technology Readiness Level (TRL) 6 by Preliminary Design Review (PDR). NASA Systems Engineering Handbook (NASA SP-2016-6105 Rev 2 2016) states that *a high-fidelity system/component prototype. that adequately addresses all critical scaling issues is built and operated in a relevant environment to demonstrate operations under critical environmental conditions is necessary* for technology to be rated at TRL 6 (NASA 2016).

The following subsection of this paper describes the manufacturing and integration of a scalable engineering development unit. Aerothermal, thermo-structural and structural tests at critical conditions are summarized, and comparisons with analytical predictions are provided.

2.3 Prototype or Engineering Test Unit (ETU)

The size of a single piece of HEEET material is limited by the width of the loom. Weaving results in flat panels and so molding the flat panels to conform to the shape of the heatshield is a required step. The width limitation requires a multiple tile architecture. Currently the maximum width is about 60 cm, so a 1 m diameter heatshield requires integration of multiple tiles. The tiled layout concept is shown in Fig. 4.

Under thermal and mechanical loading, from launch to entry, compatibility is required between TPS and the structure underneath in order to avoid structural failures. Hence a

Fig. 5 Full scale (1 m diameter) integrated engineering test unit (ETU). The nose tile, two rows of circumferential tiles, circumferential and radial seams between the acreage tiles and closeout plugs are all integrated to form the heatshield

seam that provides compliance for the integrated heatshield system is needed. In addition, the seam should have recession behavior and conduction that is very similar to the acreage. A seam material was invented, by modifying the acreage material through creation of microcracks in the phenolic resin that increase compliance with little change in density. A narrow (2.5 cm) strip of this softened material is used (see Fig. 4) as gap filler. The integration of the seam with the acreage requires complex machining and bonding operations, which have been developed, tested at sub-scale and then demonstrated at full scale. Formal procedures were developed and documented for all production steps.

All piece parts for the prototype hardware were fabricated by industry, to assure that the work instructions would adequately control part consistency. Acceptance criteria and CT scan inspection assured quality of parts that underwent testing. The HEEET ETU shown in Fig. 5 went through numerous structural tests, and the data collected were compared with analytical predictions.

2.4 Aerothermal Testing and Analysis

Aerothermal and thermo-structural tests cannot be performed on the full-scale heatshield, because facilities can apply relevant heating only on small test articles (Venkatapathy et al. 2009). For these smaller articles, the same production approaches for assembly of gaps and seams were applied, to assure consistency of behavior for the integrated system.

Assessment of HEEET's thermal response predictability relies on arcjet testing of HEEET coupons and subassemblies, to show that: (1) the material does not fail at conditions that are suitably margined beyond those expected in flight for relevant missions, and (2) the material thermal response is predictable, with acceptable fidelity, by computational

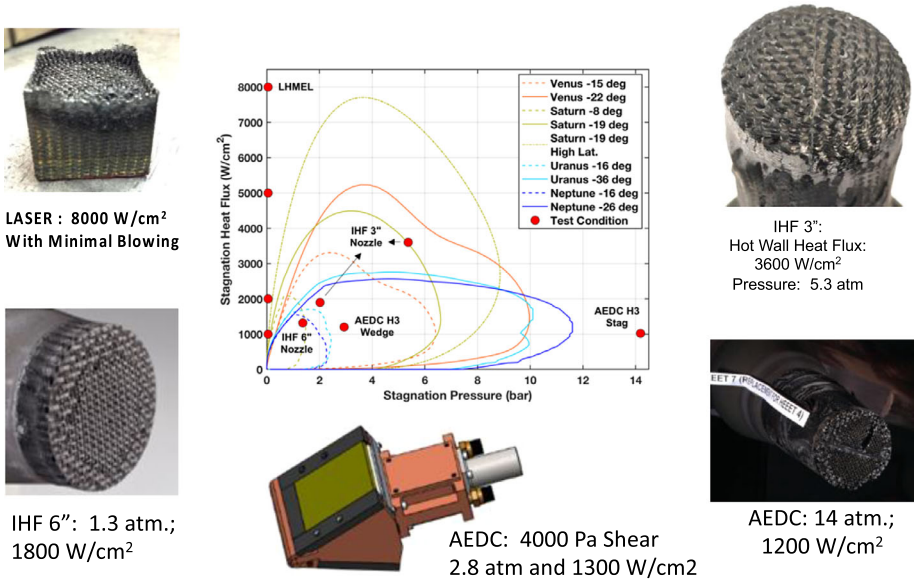

Fig. 6 Identifies the facilities, the test conditions and the corresponding test article geometry used in aerothermal testing. Testing included both LHEML, a laser test facility as well as arc jets at both NASA Ames Research Center and AEDC. The line plots show the entry environment for exploratory trajectories used to define test conditions

tools used in heatshield design. This assessment must be done for both the acreage material and seams. Due to limitations in flight-like ground testing capability, qualification of HEEET is achieved by piecing together evidence from multiple ground tests, none of which fully bound the flight conditions and vehicle configuration. Facilities were pushed to their limits and small test coupons had to be employed to achieve the desired heating conditions. The small coupons increased the challenges of data interpretation. Table 2 lists all the arcjet tests completed by the HEEET project. The table includes test conditions (hot wall), coupon geometry/size and number of coupons for each test series.

Figure 6 shows the test article geometry at different facilities, and the corresponding test conditions. The figure also includes anticipated entry environment for bounding missions at Venus, Saturn, Uranus and Neptune, in terms of the peak stagnation point heat flux and pressure along the entry trajectory. Arc jet testing does not permit us to test along these trajectories but only at discrete points. Testing at LHEML with laser heating does not involve flow around the model. The LHEML tests investigated failure modes that might be induced by heating alone.

The HEEET acreage material did not fail in any of the arcjet tests conducted by the project, showing robustness against mission-relevant environments. Therefore, the focus of TRL assessment for tiles is the predictability of the acreage material's thermal response. Figure 7 compares recession predictions from FIAT (Chen and Milos 1999; Milos and Chen 2013, and Milos et al. 2017) as a function of test duration with measurements obtained from two separate test series in the Interactive Heating Facility (IHF) arc jet at NASA Ames, with a 3" nozzle. Recession measurements are within the prediction uncertainty bounds (shown as dashed lines), which are based on uncertainty in test environments.

Testing stagnation coupons does not account for shear effects, so wedge models were tested at AEDC, in an environment with lower pressure and heat flux but flight-relevant

Table 2 List of all the arcjet tests completed by the HEEET project

Test date	Facility	Heat flux (W/cm^2)	Pressure (atm)	Shear (Pa)	Enthalpy (MJ/kg)	Sample size (mm)	Sample shape	Test gas	TC instrum.	Acreage coupons	Seam coupons
2013-Aug	IHF76 mm nozzle	2500	5.3	0	23.4	25	Flat Face	Air	None	4	0
2014-Apr	LHMEL	8000	0	0	N/A	25×25	Flat Face	N2	BackFace	2	0
		5000	0	0	N/A	25×25				2	0
		2000	0	0	N/A	51×51				2	0
		1000	0	0	N/A	51×51				2	0
2014-Mar	AEDC Stag	1025	14.5	0	11.6	51	Flat Face	Air	None	1	0
2014-Oct	AEDC Wedge	1200	2.9	4000	11.6	102×127	Wedge	Air	BackFace	2	12
2015-Feb	AHF305 mm nozzle	80	0.03	0	12.2	102	IsoQ	N2	TC Stack	2	0
		62					Flat Face			2	0
		220	0.12		16.7		IsoQ			2	0
		170					Flat Face			2	0
2015-May	IHF152 mm nozzle	1025	1.35	0	24.8	51	Flat Face	Air	None	0	10
2015-Nov	IHF76 mm nozzle	3600	5.3	0	23.4	25	IsoQ	Air	None	8	12
2016-Aug	AEDC Stag	1025	14.5	0	11.6	51	Flat Face	Air	None	1	2
2016-Aug	AEDC Wedge	1200	2.9	4000	11.6	102×127	Wedge	Air	BackFace	2	6
2016-Aug	IHF330 mm nozzle	280	0.31	0	21.2	152	Flat Face	Air	TC Stack	2	2
		150	0.13	0	17.3					2	2
2018-Mar	IHF152 mm nozzle	1320	1.35	0	21.3	51	IsoQ	Air	None	1	0
2018-May	AEDC Wedge	1200	2.9	4000	11.6	102×127	Wedge	Air	BackFace	2	16
2018-Jun	IHF76 mm nozzle	1900	2.0	0	20.2	25	IsoQ	Air	None	3	3
		3600	5.3	0	23.4					3	17
2019-Jul	AEDC Wedge	1200	2.9	4000	11.6	102×127	Wedge	Air	BackFace	7	7
									Total	54	89

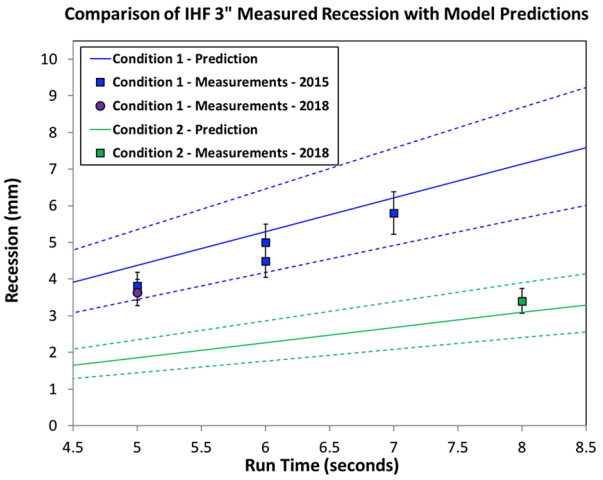

Fig. 7 Comparison of measured and predicted recession for HEEET acreage material tested in the AEDC arcjet

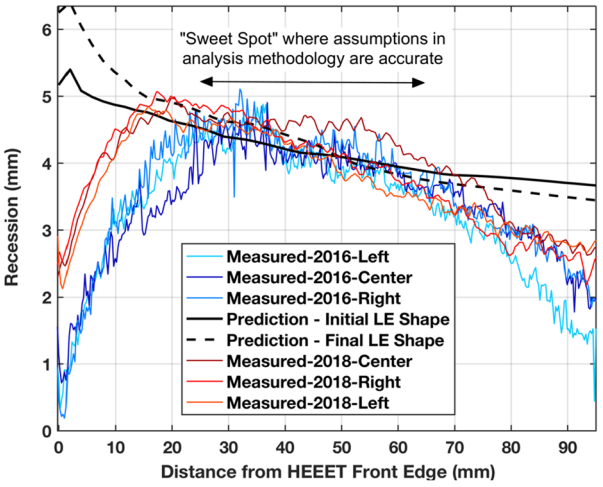

Fig. 8 Comparison of predicted and measured recession from the wedge configuration tests conducted in the AEDC arcjet facility in 2016 and 2018

shear. In Fig. 8, recession predictions are compared with measurements obtained from two wedge test series conducted at AEDC. This is a very complex test as the leading edge recedes in time, which changes the flow on the wedge. Recession along the running length of the wedge for three different cross-sections (center, left and right) is shown. The black lines show FIAT recession predictions based on CFD-predicted environments on the wedge centerline. The dashed black line attempts to account for the impact of leading-edge erosion and shape change on the wedge environments. The complexity of the flow field, which includes impingement of expansion fans that originate from the nozzle's edge and interaction between the wedge leading edge and the upstream section of the model, limits validity of current predictions to a "sweet spot" region in the middle of the wedge.

A few stagnation coupons were tested at extremely high (∼14 atm.) pressure. Recession measurements at these conditions were higher than model predictions, indicating that the material was being removed by mechanisms other than simple thermochemical ablation of solid carbon, which may have been initiated (or exacerbated) by non-flight-like geometry of the test article where extreme pressure gradients near the edge of the article can encourage

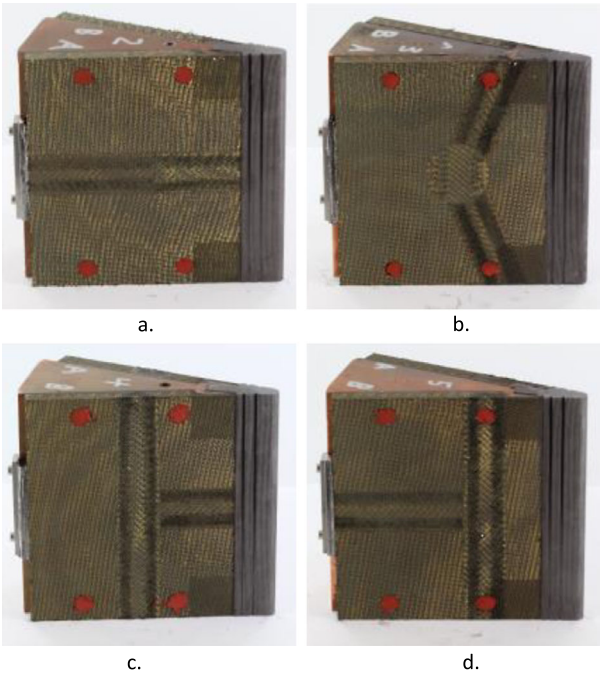

Fig. 9 AEDC arcjet seam configurations: a. Radial, b. Circumferential—Circumferential joint with closeout plug, c. Radial—Circumferential (upstream T) and d. Circumferential—Radial (downstream T)

flow penetration and mechanical removal. Since the behavior is not adequately explained, HEEET is not at TRL 6 for these conditions. Although the recession exceeded predictions, it was steady and no run-away failure mode was observed in repeated testing.

A number of seam features exist on the full-scale heatshield (Fig. 5). All seam features were tested in wedges at the AEDC facility, and typical models are shown in Fig. 9. A few areas of localized opening of the adhesive were observed post-test, but no associated evidence of augmented in-depth heating was found. Short running lengths of very narrow openings do not constitute a runaway failure mode.

No thermal response model was developed for the seam gap-filler and adhesive. The variation in recession augmentation observed across the different tests as well as within a given test article, ranges from ∼11% to ∼51%, with most measurements in the 20–40% range. Recession rate does not accelerate during tests, so there is no indication of runaway behavior. A margin policy can be applied to provide total thickness that accounts for higher recession at the seams. The predictability of aerothermal behavior for prototype seams tested at mission-relevant conditions is sufficient to rate Technology Readiness at Level 6.

2.5 Thermo-structural Testing and Analysis

The structural testing must cover all phases of the mission from launch through entry. The structural test campaign consisted of three basic types of testing: (i) element level testing, such as mechanical and thermal material properties of the individual layers as a function of temperature; (ii) sub-component testing, such as 4-point bend testing of coupons, both acreage and seams; and lastly, (iii) subsystem testing, or testing of the ETU, which is in essence a Saturn probe prototype that is at a relevant scale, and was built with the materials and processes developed for use on a flight vehicle. The ETU testing verified the structural design tools at relevant scale and was used to determine any issues with workmanship.

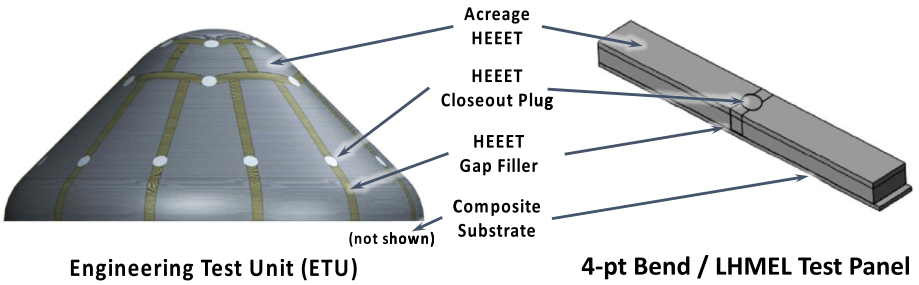

Fig. 10 The four-point bend test structural test article used in the LHMEL facility shown on the right side. This test article represents a simplified region of the full-scale ETU (shown on the left) consisting of acreage, seam and closeout plugs

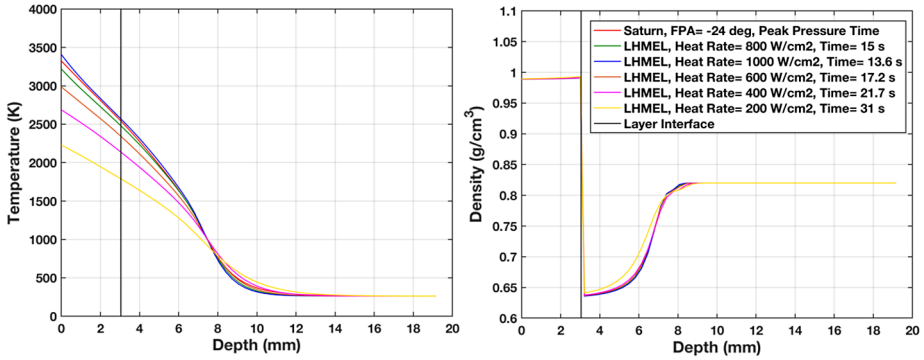

Fig. 11 Comparison of temperature and density profiles for a representative Saturn entry case, at the time of peak pressure

It is exceedingly difficult to test combined loading that is representative of entry conditions, particularly for entries that involve extreme heating rates. The four-point bending fixture, shown in Fig. 10 was developed for the LHMEL facility. To test a seam that is on the order of 2.5 cm width, a heating area of several centimeters is needed. At the LHMEL, an elliptical spot size of about 18 cm (major axis) and 10 cm (minor axis) can apply around 90 W/cm^2, which is a small fraction of mission-relevant rates. Although the temperature gradient is lower than flight, the material state can still be representative of flight. The plot on the left side of Fig. 11 shows the temperature gradient through the thickness of the material for various laser power level in comparison to expected in flight for a Saturn mission. On the right side of Fig. 11, the density profile as a function of depth shows the material decomposition results in char and hence all of the profiles collapse to a single density profile. Hence, at a uniform laser heat flux of 90 W/cm^2 over 18 cm $\times$ 10 cm area, a long duration exposure can provide a flight relevant material state.

With the four-point bend fixture, the panels can be pre-loaded to a percentage of the room temperature load capability, and then held at fixed displacement while heating is applied. The load level drops during testing, but so does the system capability, as the charred adhesive loses load-carrying capability. Most of the resistance to gap opening is provided by the remaining virgin adhesive. If an initial load level does not induce failure even after the recession layer is fully charred, the system should be capable of surviving that level

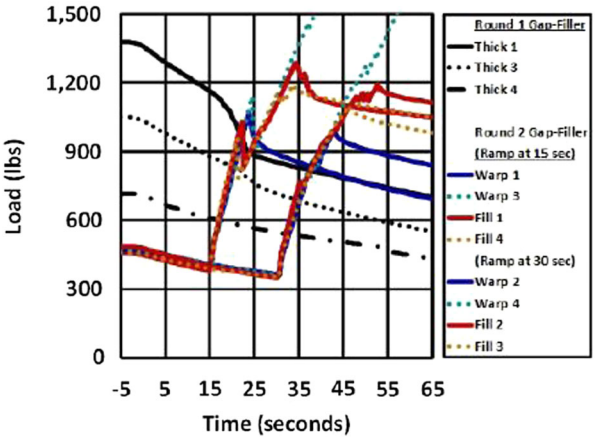

Fig. 12 Load histories for fixed displacement (black traces) and increasing displacement (colored traces) during heating pulse

of displacement for any representative density gradient through the recession layer (from virgin all the way through the thickness to fully charred all the way through the recession layer).

Results for three different levels of pre-loaded fixed bending displacement are shown in black in Fig. 12. Without strong statistics, it is reasonable to conclude that, for this test article configuration, initial loading above 5600 N is likely to induce gap opening as the recession layer chars, while loading to only 4600 N does not cause gap opening even when the recession layer is fully charred. Subsequent testing attempted to apply load in a more flight-like manner. Since the pressure pulse typically lags the heating pulse, the test articles were initially lightly loaded in bending, and then displacement was increased during the heating pulse. Two different time delays were used prior to ramping the bending displacements through the four-point fixture, as shown by colored traces in Fig. 12. None of the specimens loaded in this manner failed at a load lower than the specimen that had fixed displacement with 3100 N of initial load. All samples continued to carry load after initial adhesive failure, indicating that gap opening typically did not propagate deeper than the transition layer.

Finite-element analysis of the joint indicates that the 3100 N initial loading causes a little more than 0.5 mm of gap-filler expansion at the outer mold line. Hence there is strong evidence that seams are capable of carrying 0.50 mm of gap-filler expansion throughout an entry heating pulse. Similar testing for panels with closeout plugs showed no failure below 0.23 mm of displacement; the plugs are known to be stiffer than the gap-filler so the lower capability is unsurprising. If a 30% knockdown is applied, to account for the small number of tests, a design allowable of 0.15 mm of gap-filler expansion can be prescribed. Reasonable structural substrate designs require less than 0.075 mm of expansion, so a gap-filler placed at the most demanding location on the heatshield would have structural margins on seam displacement greater than 2. This level of demonstrated capability supports a finding that HEEET is TRL 6 with respect to combined loading in entry environments.

2.6 Structural Testing and Analysis at Full Scale

Relevant environments for structural testing include launch and ascent loads (vibration and acoustics), in-space thermal and vacuum loads, and pressure loading during entry. The test load cases that address these mission cases, and associated inspections, are summarized

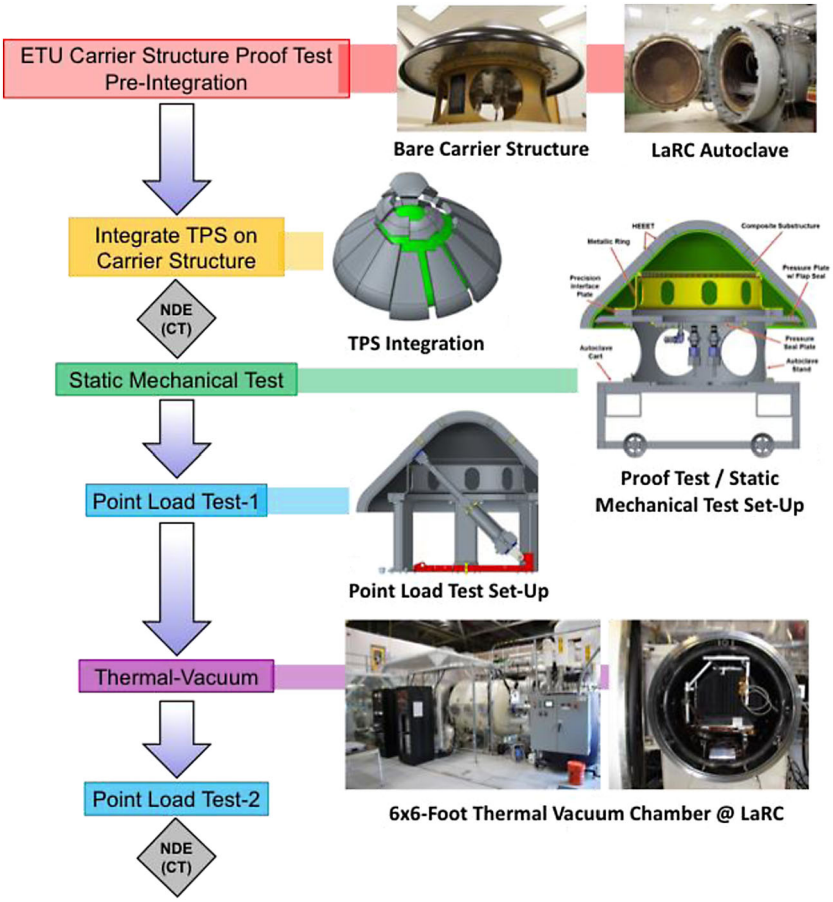

Fig. 13 Test and inspection sequence for 1 m diameter heatshield Engineering Test Unit

in Fig. 13. Vibration testing was originally planned, but eliminated from the test program because analysis showed loads were bounded by other test cases. The data used for model correlation are strain measurements at distributed locations across the test article.

A FEM model was used for post-test analysis of ETU static pressure and point load tests. Strains typically matched with $\pm 15\%$ at most locations. Larger discrepancies, up to about 30%, were observed in regions where forming has modified local properties of the HEEET material. It would be possible to improve predictive accuracy by testing more curved components to establish more accurate properties, but such effort was not warranted, because large positive structural margins could be achieved even with the uncertainty in material properties in regions of high curvature. Correlation was not attempted for the thermal vacuum test because measured strains were relatively small, so percentage measurement errors limit the quality of correlation. The inspection program confirmed that the Engineering Test Unit survived mission-relevant loads without significant damage progression.

Based on testing of a fully relevant prototype to design load levels, successful correlation of design models, and post-test inspection, the HEEET system is at TRL 6 for all mission load cases prior to entry.

2.7 On the Scalability of the Design from ETU to Flight

The size of the entry system for Ice Giants Probes (IGP) could range from 1.0 m up to 1.5 m diameter (Tauber 1971; Swenson et al. 1990, Hofstadter 2017, and Hwang 2018). The manufacturing and integration of the 1 m diameter ETU utilized the 30.5 cm (12 inches) wide woven preforms. NASA has currently established weaving capability up to 61 cm (24 inches) width. The ETU arrangement with the nose cap and two rows of tile was chosen so that this architecture can be scaled up to 5 m size if needed. IGP missions are expected to be limited to 1.5 m or less and do not present any challenge in terms of area scalability. If the required thickness scaling of insulating and recession layers exceeds the thicknesses that have been demonstrated, then the current weaving capabilities would need to be enhanced and integration of the thicker material would need to be demonstrated. In a later section the mission and design constraints due to thickness capability is addressed.

HEEET development included verification of tools such as TPS sizing, thermo-structural analysis and structural design tools. The tools that were used in the design and analysis of the element, component, sub-system and system tests were the tools that NASA has developed and applying for various missions, such as MSL, Orion, Mars 2020, and OSIRIS-REx, adapted to reflect the relevant properties of the HEEET material. Correlation with ground test data for HEEET validates the use of these tools for design of ICP missions. While the tools are applicable, verification of the point-design flight TPS should involve testing using ground test facilities. Test facility limitations will impose constraints on the flight design, if verification at bounding environments is required. This is also addressed in a later section.

3 Ice Giants Probes

The two latest studies (Hofstadter et al. 2017 and Hwang 2018) show that, depending on requirements and choices, entry environments van vary widely. Therefore, in evaluating HEEET, for Ice Giant Missions, the impact of design parameters in terms of manufacturing as well as flight certification risks need to be considered in early mission design.

Early in the development of HEEET, thickness sizing studies were conducted, using measured properties of the dual layer weave, for several destinations and several entry trajectories for each destination. More recently the study performed by the common probe project (Hwang 2018) for probe mission at Venus, Saturn, Uranus and Neptune used the same entry system for all missions. The entry flight path angles at Venus, Saturn, Uranus and Neptune were kept low in order to achieve low deceleration load. The study estimated the mass for HCP and HEEET. Results from this study are shown in Fig. 14. The TPS mass estimate comparisons between HCP and HEEET across all destinations show that HEEET is more mass efficient than HCP (mass savings $>40\%$).

To understand whether HEEET is acceptable for a specific mission opportunity, two primary questions that need to be answered are: (i) will the required thickness of the TPS exceed the demonstrated manufacturing capability, especially for shallow entries? and (ii) will the required environment exceed the range for which HEEET is considered safe and viable based on ground test data, especially for steep entries?

The TRAJ code (Allen et al. 2004), which is designed to perform early trade studies including TPS sizing, was used in both pre-decadal study and the common probe study. It constructs a 3DOF trajectory for a given entry state and entry ballistic coefficient for a given planet. Based on the trajectory and atmospheric conditions, it estimates stagnation conditions such as heat flux, pressure, and g-load, and integrates the heat flux to calculate

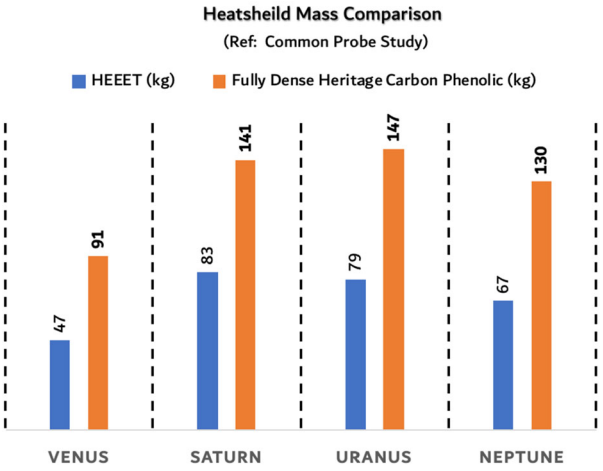

Fig. 14 Heatshield mass Comparison of Heritage Carbon Phenolic and HEEET at Venus (CO_2), Saturn (H_2/He), Uranus (H_2/He) and Neptune (H_2/He) for a common entry system (Hwang 2018)

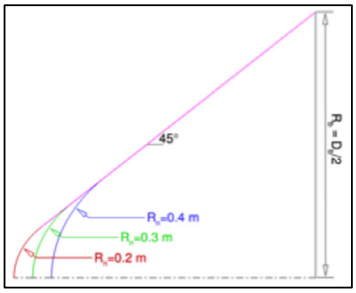

β kg/m^{-2}	D_b 1.0 m	D_b 1.2 m	D_b 1.4 m
	Mass (m)/kg		
200	165	238	323
250	206	297	404
300	247	356	485
350	289	416	566

Fig. 15 Range of nose radius and ballistic coefficient used to illustrate the entry environment and perform HEEET sizing studies

total integrated heat load. The TRAJ code has sizing analysis built in for numerous TPS materials including HEEET. This tool is utilized to answer the above two questions.

A variational study was conducted to evaluate the peak stagnation conditions for three nose radii and four ballistic coefficients, with chosen values for these parameters shown in Fig. 15.

Results for entry environment for Uranus and for Neptune are shown in Figs. 16 and 17, respectively. Thousands of trajectory computations were performed to generate the plots shown. The key observations from these simulations are as follows:

1. For the range of ballistic coefficients considered, g-load depends primarily on entry flight path angle for both Uranus and Neptune. G-load is lower for shallower entry (lower) flight path angles.
2. The heat load is a strong function of entry flight path angle and weakly dependent on ballistic coefficient. Heat load is higher for shallower entry for a given ballistic coefficient. For a given entry flight path angle, the higher ballistic coefficient correlates with the higher heat load.
3. The peak stagnation heat flux and pressure behave very similarly and are dependent on both entry flight path angle and ballistic coefficient. In general, for any given entry flight

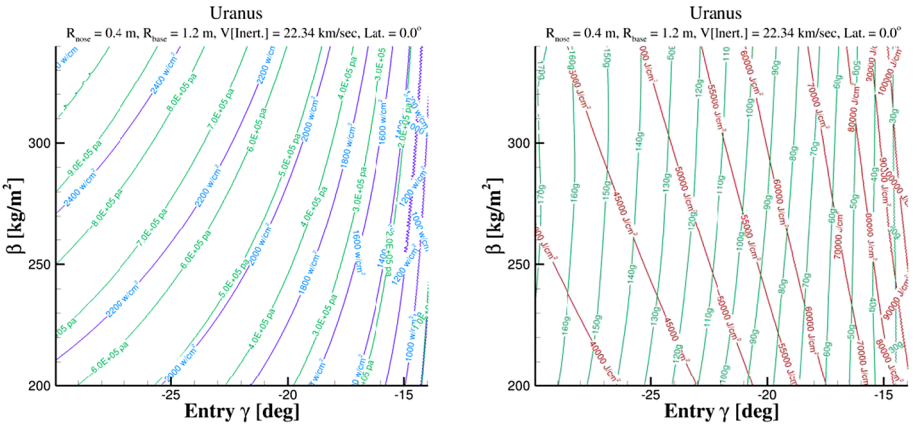

Fig. 16 Stagnation point peak heat flux and pressure (left), and g-load and total stagnation point heat load(right) for a range of ballistic coefficients and entry flight path angles for Uranus entry (for a fixed nose radius, base radius and entry velocity)

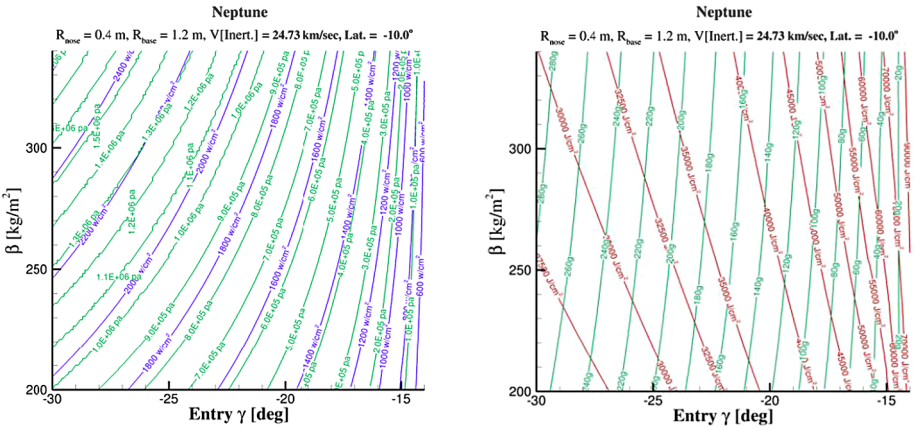

Fig. 17 Stagnation point peak heat flux and pressure (left), and g-load and total stagnation point heat load(right) for a range of ballistic coefficients and entry flight path angles for Neptune entry (for a fixed nose radius, base radius and entry velocity as shown in the plots)

path angle, higher ballistic coefficient results in higher heat flux and pressure. For a given ballistic coefficient, lower entry flight path angle, lowers both the heat flux and pressure.

4. For Uranus, for the range of entry flight path angles and ballistic coefficients considered, the heat flux and pressure can range from (1000 W/cm^2, 1 atm) at $-15°$ entry flight path angle and 200 kg/m^2 ballistic coefficient up to (2500 W/cm^2 and 10 atm) at $-30°$ entry flight path angle and 350 kg/m^2 ballistic coefficient.
5. Higher entry velocity will result in higher heat flux, pressure, g-load and heat load (not shown here, but simulations were performed to bound the environment).

Figure 18 provides a summary from the above study on a log-log scale, and represents the potential entry environment that needs to be considered in evaluating HEEET for both Uranus and Neptune. The IGP entry environments are represented by two groups of ellipses.

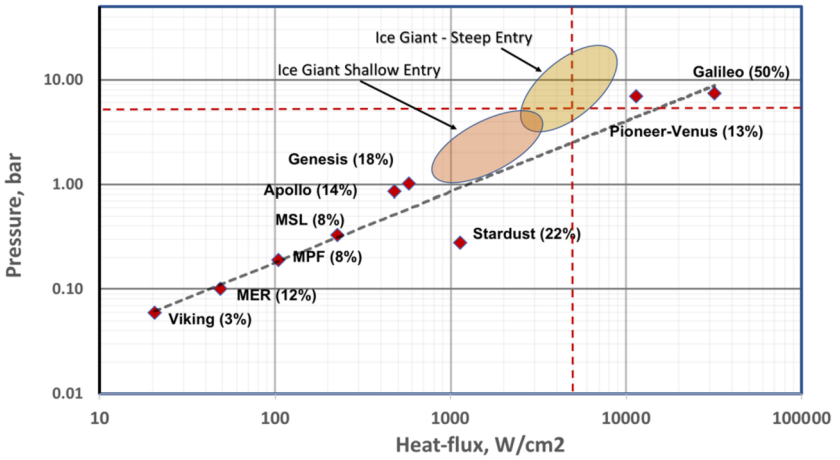

Fig. 18 The range for peak stagnation heat flux and pressure for Ice Giant entry in comparison to other missions flown. The ground test facility limitations are expressed as dotted red line in terms of heat flux and pressure achievable

The dotted red line represents the limit of heat flux and pressure that HEEET has been tested in arc jet test facilities (with limited extrapolation). If IGP missions can remain below peak stagnation pressure of 5 atm. and below peak stagnation heat flux of 3600 W/cm^2, HEEET is well suited. For conditions higher than (5 atm, and 3600 W/cm^2), while HEEET may be applicable, inadequate ground test data and the challenges of future flight certification represent a potential mission risk.

4 Concluding Remarks

The HEEET project has generated a wealth of data for a new, innovative, scalable TPS architecture that is based on 3D weaving technology. Technology readiness has been demonstrated by building a 1 m (diameter) proto-flight/engineering test unit, and by demonstrating design tools have the fidelity needed for flight design through correlation of analytic predictions with aerothermal, thermal and thermomechanical test data. Extensive documentation captured during the development will support infusion of HEEET into missions.

Any design is a compromise between various elements. It also represents balance between risks across many disciplines. Heatshield constraints with HEEET are well characterized. The majority of the Uranus and a large set of Neptune mission options are shown to be feasible and enabled by HEEET. Options to further expand the HEEET capability should be considered especially for missions to Ice Giants, if the HEEET constraint pushes the design into unacceptable risk or a configuration that does not close. Ice Giant Probe missions are enabled as a result of HEEET development and delivery of TRL 6 technology.

Acknowledgements The HEEET project is grateful to NASA's Space Technology Mission Directorate, the Game Changing Development Program and the Planetary Science Division, Science Mission Directorate for their support. Any endeavor of the magnitude of HEEET requires the support of a large number of folks within the agency, primarily at NASA's Ames, Johnson and Langley centers, that deserve acknowledgment, and are too many to name here. The project gratefully acknowledges the arcjet complex at NASA Ames Research Center, the High Enthalpy Arc Heated facilities at Arnold Engineering Development Complex in Tullahoma,

TN and the Laser Hardened Materials Evaluation Laboratory (LHMEL) at Wright Patterson Airforce Base in Dayton OH. The industrial partners, Bally Ribbon Mills Inc of Bally, PA and Fiber Materials Inc. of Biddeford, ME were invaluable. The Independent Review Board (IRB) provided continual critical review and feedback from the beginning to the end of the project and eventually certified that HEEET achieved TRL 6, and so the project extends its appreciation to the members of the IRB: Prof. Robert Braun of University of Colorado, Boulder (chair); Robin Beck, NASA ARC; Pam Hoffman, NASA JPL; Christine Szalai, NASA JPL; Stan Bouslog, NASA JSC; Michael Amato, NASA GSFC; Anthony Calamino, NASA LaRC; Michelle Munk, NASA LaRC; Ken Hibbard, Johns Hopkins University, Applied Physics Laboratory; and Steve Gayle, NASA LaRC. The project is thankful to the management at NASA Centers and the organizations mentioned above for their continued support through the duration of the project.

References

P. Agrawal, G.A. Allen Jr., E.B. Sklyanskiy, H.H. Hwang, L.C. Huynh, K. McGuire, M.S. Marley, J.A. Garcia, J.F. Aliaga, R.W. Moses, Atmospheric entry studies for Uranus. IEEE Aerosp. Conf. Proc. (2014). https://doi.org/10.1109/AERO.2014.6836417

G.A. Allen Jr., M.J. Wright, P. Gage, The Trajectory Program (Traj): Reference manual and user's guide (2004). NASA TM-2004-212847

S.K. Atreya, S. Bolton, T. Guillot, T.C. Owen, Multiprobe exploration of the giant planets–shallow probes, in *3rd International Planetary Probe Workshop (also ESA Special Publication WPP263)* (2006)

Y.K. Chen, F.S. Milos, Ablation and thermal response program for spacecraft heatshield analysis. J. Spacecr. Rockets **36**(3), 475–483 (1999). https://doi.org/10.2514/2.3469

M. Hofstadter, et al., Ice Giant Pre-Decadal Mission Study Report, Pre-decadal Survey Mission Study Report, Prepared by Solar System Exploration Directorate Jet Propulsion Laboratory for Planetary Science Division Science Mission Directorate NASA, June 2017, JPL-D 100520. https://www.lpi.usra.edu/icegiants/mission_study/Full-Report.pdf

W.B. Hubbard, Appendix G 23: Uranus orbiter and probe mission concept study, in *Visions and Voyages for Planetary Science in the Decade 2013–2022* (National Academies Press, Washington, 2011). https://doi.org/10.17226/13117

H.H. Hwang, A Common Probe Design for Multiple Planetary Destinations, presented at the 16th Meeting of the Venus Exploration Analysis Group (VEXAG) meeting, Nov. 2018. https://www.colorado.edu/event/ippw2018/sites/default/files/attached-files/aeroentrytech_12_hwang_presid578_presslides_docid1131.pdf

S. Mezines, Carbon phenolic heat shields for Jupiter/Saturn/Uranus entry probes, in *Proceedings of the Outer Planet Probe Technology Workshop* (NASA Ames Research Center, Moffett Field, 1974), VI-2-13

F.S. Milos, Y.K. Chen, Ablation, thermal response, and chemistry program for analysis of thermal protection systems. J. Spacecr. Rockets **50**(1), 137–149 (2013). https://doi.org/10.2514/1.A32302

F.S. Milos, Y.K. Chen, M. Mahzari, Arcjet tests and thermal response analysis for dual-layer woven carbon phenolic, in *AIAA Paper 2017-3353, 47th AIAA Thermophysics Conference* (2017). https://doi.org/10.2514/6.2017-3353

NASA, Appendix G.4, in *NASA Systems Engineering Handbook*, NASA SP-2016-6105 Rev 2 (2016). https://www.nasa.gov/sites/default/files/atoms/files/nasa_systems_engineering_handbook_0.pdf

National Research Council (NRC), *Vision and Voyages* (National Academies Press, Washington, 2011). https://doi.org/10.17226/13117

R.J. Sullivan, J.I. Waters, J.H. Dunkin, First generation atmospheric probes (10-BARS) for Uranus and Neptune, NASA CR-129815 (also Report M-34, Astro Sciences, IIT Research Institute, Chicago) (1972). https://ntrs.nasa.gov/search.jsp?R=19730005097

B.L. Swenson, P.F. Wercinski, R.T. Reynolds, A.C. Mascy, Deep atmospheric probe missions to Uranus and Neptune, in *AIAA Paper 90-2893-CP, AIAA/AAS Astrodynamics Conference*, Portland, OR, August 20–22, 1990 (1990). https://doi.org/10.2514/6.1990-2893.

M.E. Tauber, Heat protection for atmospheric entry into Saturn, Uranus, and Neptune, in *AAS Paper 71-145, 17th Annual Meeting on Jupiter Orbiters and Probes—A Preliminary Assessment of Requirements*, Seattle, WA, June 28–30, 1971 (1971). https://ntrs.nasa.gov/search.jsp?R=19710057251

M. Tauber, P. Wercinski, W. Henline, J. Paterson, L. Yang, Uranus and Neptune atmospheric-entry probe study. J. Spacecr. Rockets **31**(5), 799–805 (1994). https://doi.org/10.2514/6.1993-3689

E. Venkatapathy, B. Laub, G.J. Hartman, J.O. Arnold, M.J. Wright, G.A. Allen Jr., Thermal protection system development, testing, and qualification for atmospheric probes and sample return missions: examples for Saturn, Titan and Stardust-type sample return. Adv. Space Res. **44**(1), 138–150 (2009). https://doi.org/10.1016/j.asr.2008.12.023

N. Vojvodich, R. Reynolds, T. Grant, P. Nachtsheim, Outer planet atmospheric entry probes-an overview of technology readiness, in *AIAA/AGU Conference on the Exploration of the Outer Planets*, St. Louis, MO (1975). https://doi.org/10.2514/6.1975-1147

P. Zell, E. Venkatapathy, J. Arnold, The block-ablator-in-a-honeycomb heat shield architecture overview, in *International Planetary Probe Workshop*, vol. 7 (2010), pp. 12–18